Journal of *Marine Science and Engineering*

MDPI

Article

Potential Influence of Offshore Wind Farms on the Marine Stratification in the Waters Adjacent to China

Zhan Lian [1,2,3,*], Kun Liu [1] and Tong Yang [1]

[1] Institute of Marine Science, Guangdong Provincial Key Laboratory of Marine Disaster Prediction and Prevention, Shantou University, Shantou 515063, China
[2] State Key Laboratory of Marine Environmental Science, Xiamen University, Xiamen 361102, China
[3] Laboratory for Regional Oceanography and Numerical Modeling, Pilot National Laboratory for Marine Science and Technology (Qingdao), Qingdao 266237, China
* Correspondence: zhanlian@stu.edu.cn

Abstract: Offshore wind farms (OWFs) can influence marine stratifications, leading to fuel nutrition in the upper ocean and regulating ocean carbon fluxes. Evaluating this dynamic effect facilitates the planning of OWFs deployment for enlarging marine carbon sequestration, which is urgent in the pursuit of China's carbon neutrality targets. However, it is impossible to observe the target influence in the planning stage of deployments, and it is impractical to build a high-resolution (10^0~10^1 m) model to cover the entire waters adjacent to China. The theoretical calculations, therefore, are the first step and top priority. The simplified theory presents two suggestions in the design of future OWF deployments in the study area. The first suggestion is made from the perspective of OWF positioning. To the east of the cities of Zhoushan, Putian, and Shantou, the oceans are dynamically sensitive to OWF deployments. The second suggestion is made from the perspective of the length scale of OWFs. A broader OWF results in a smaller vertical disturbance in the coastal waters, but the situation is opposite in the open seas. The OWF deployment strategy, proposed in the aim of ensuring idealized marine stratification responses, thus varies geographically. This study provides a panoramic view of the sensitivity of marine stratification to OWFs in the study regions. It can be seen as a steppingstone in detailed research of the target phenomenon.

Keywords: offshore wind farm; seawater vertical movement; marine stratification; development strategy; adjacent water of China

Citation: Lian, Z.; Liu, K.; Yang, T. Potential Influence of Offshore Wind Farms on the Marine Stratification in the Waters Adjacent to China. *J. Mar. Sci. Eng.* **2022**, *10*, 1872. https://doi.org/10.3390/jmse10121872

Academic Editor: Christos Stefanakos

Received: 26 October 2022
Accepted: 11 November 2022
Published: 3 December 2022

1. Introduction

Wind energy is a virtually carbon-free electricity source. Accordingly, many coastal regions are turning to offshore wind energy technologies to meet rising energy demands. The low carbon footprint of offshore wind energy is essential in reducing global carbon emissions and mitigating the climate crisis [1–3].

Offshore wind farms (OWFs) play an important role in regulating the marine ecosystem [4] and carbon flux [5,6], which might further amplify the low-carbon features of offshore wind energy technologies via enhancing marine carbon sequestration. In stratified waters, vertical seawater velocity and the corresponding changes in stratification are the key factors influencing the target phenomenon [7]. The vertical motion of seawater can transport nutrition to the upper sea, thus regulating marine productivity [8,9]. OWFs are presently being built or planned in regions which are deep enough to be seasonally stratified [10]. Therefore, it is urgent that we evaluate the influences of OWFs on marine stratification.

The wind wake of OWFs is induced by the wind speed deficit in the leeward side of wind turbines [11–14], and it results in upwelling/downwelling currents in the affected area [15]. This can be explained by geophysical fluid dynamic theory. When a wind farm is large, and when atmospheric stratification is stable, offshore wakes may extend to several

dozens of kilometers downstream, as shown by a number of observations [16,17] and numerical investigations [18,19]. Here, the length scale is big enough to be well suited for geophysical fluid dynamic theory [20,21]. According to Ekman theory, this spatial pattern of wind stress forces sea water to move vertically (Figure 1) [22]. Neglecting some effects (such as small-scale mixing, friction, and secondary circulation), the maximum vertical velocity can be estimated by a reduced-gravity model. The theoretical estimation has been verified by an ocean general circulation model with fine resolution (200 m × 200 m horizontal measurements and 0.5 m vertical measurement) and a constant water depth (20 m) [15]. Such wake-induced upwelling/downwelling has been confirmed by other idealized models [23–25]. A simulation showed that the upwelling/downwelling can measure up to 3–4 m per day in the North Sea [20]. This magnitude is sufficient to dramatically influence local marine stratification and, more importantly, can influence primary production and marine carbon flux [26]. Most recently, the presence of an upwelling/downwelling dipole was measured in the German Bight; it was characterized in terms of changes in the mixed layer's depth [27]. Similar phenomena, induced by wind speed spatial shear, have been extensively studied at coastal boundaries [28], in seasonal upwelling areas [29], in deep waters [30], and in marginal ice zones [31].

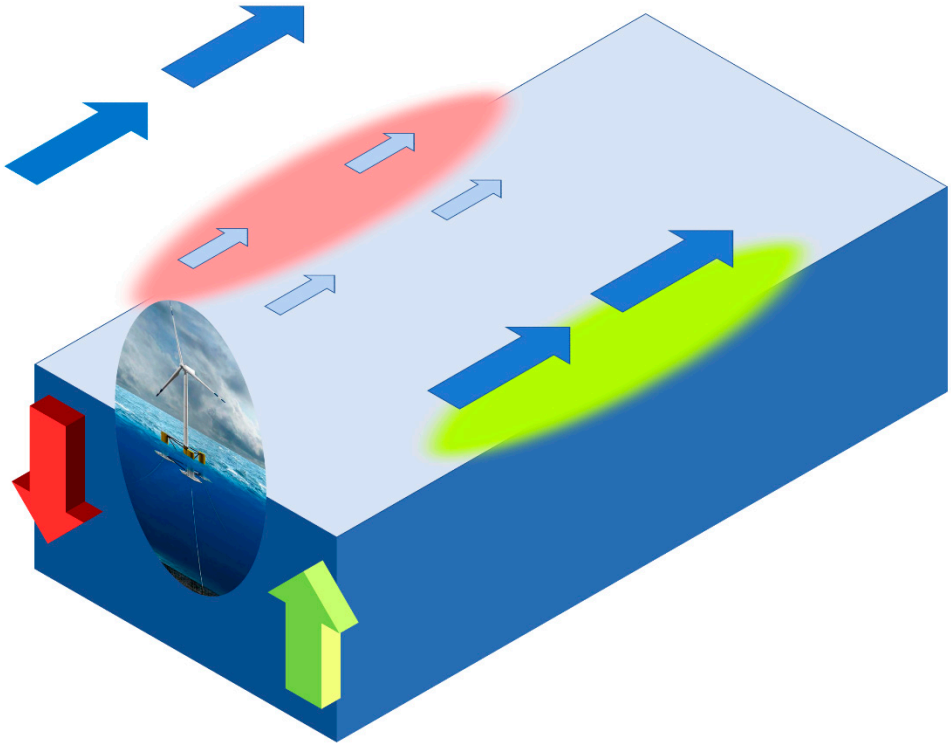

Figure 1. Schematic diagram for the mechanism of marine vertical response to the wind-forcing deficit on the leeward side of a wind turbine. The blue arrows indicate wind stress. The wind stress outside the wind turbine is undisturbed and large, but it is small behind the wind turbine due to the energy extraction. The green and red arrows represent the upwelling and downwelling currents, respectively.

There are many other wake-related effects which, in addition to the foundations of OWFs, may induce changes in marine stratification; however, they have fewer scales in comparison with the effect controlled by the Ekman theory. For instance, the wakes have impacts on air–sea heat and humidity fluxes; thus, they modulate local marine stability and climate [32]. Surface gravity waves induced by wind speed changes may also play a role in vertical mixing [33]. The piles of wind turbines can enhance small-scale turbulence [34] and generate internal waves [35]. An unstructured model and in situ observations revealed that these factors lead to changes in stratification [10] and in the marine ecosystem [26] due

to increased mixing. These effects are all relatively constrained to the sea surface or in the areas near the turbine piles. They cannot extend as far as the Ekman effect.

Estimations of marine stratification changes caused by OWFs are urgently needed in China. China has promised to begin cutting its carbon emissions within the next ten years and to become carbon neutral before 2060. To achieve this target, wind electricity production needs to show a ninefold increase in China over the next 40 years [36]. China has become one of the fastest-growing countries for offshore wind power technology development [37], and installed half of all new global offshore wind capacity in 2020 [38]. Its newly installed offshore wind power technologies will continue to increase in capacity according to the ambitious projects proposed by coastal Chinese provinces. For example, before 2030, Guangdong Province plans to increase the installed capacity of wind turbines by 50 million kilowatts in the coastal waters of Shantou City [39].

There are numerous investigations on the marine environmental effects of OWFs in China-adjacent seas [40,41]; however, there has been little focus on the stratification changes as being governed by the Ekman theory. For instance, simulations have been made for the wave–seabed–OWF interaction in the East China Sea [42]. The marine sediment quality was found to be affected by OWFs in the Bohai Sea, and the microbial communities surrounding OWFs were also influenced [43,44]. The volume of plastic in the wind farm area was lower than that outside the wind farm due to the hydrodynamic effect [45]. With a consideration for economic feasibility, OWFs should be integrated with cage aquacultures near the Taiwan Strait [46]. Biological data showed that detritus, phytoplankton, zooplankton, anchovies, and some benthic fish were positively impacted by the OWFs in the Yellow Sea [47].

Given the profound impacts of OWFs on marine environments in the waters adjacent to China, an environmentally friendly OWF deployment plan is important. There have been some assessments of OWF lifecycle environmental emissions [48,49], as well as of the geopolitical and humanistic environmental impacts [50] of OWFs in China; however, suggestions and principles for a deployment plan which will enable an idealized marine stratification response have not yet been presented. According to the Ekman theory, vertical ocean response is controlled by the length scale, the location, and the surrounding atmospheric and marine conditions of OWFs. These factors vary geographically; therefore, the OWF deployment strategy must be adjusted to achieve an idealized ocean response.

Estimating the seawater vertical velocity using the Ekman theory is necessary to propose OWF development plans which are beneficial in reducing China's carbon emissions. The reason is twofold. Firstly, it is the first step in planning OWF deployment. It is impossible to observe marine dynamic responses in the planning stages; thus, presenting a theoretical panoramic view of influencing factors is helpful in generally locating which seas are sensitive to the deployment of an OWF. Moreover, it is the top priority of numeric simulations. A high-resolution (10^0 m~10^1 m) model is necessary to comprehensively address the focus of this study [51,52]. However, it is impractical to use such a sophisticated model to cover the entire waters which are adjacent to China. Therefore, a pre-estimation of ocean responses facilitates regional model configurations. In summary, theorical estimations are very valuable; however, they are insufficient for depicting the detailed spatial patterns of vertical velocities.

In this paper, using climatological 3D ocean stratification data and wind stress data, we calculated the ocean's response to OWF deployments. We analyzed the effect of OWF locations and length scales on generating vertical seawater velocity. The rest of this paper is organized as follows. The data and methods are described in Section 2. In Section 3, we analyze the results and describe the spatial variability of the ocean vertical response to OWFs in the waters adjacent to China. Finally, the conclusions are presented in Section 4.

2. Methodology

2.1. Study Region

The bathymetry of the study region is shown in Figure 2. The cities which are seeking the development of offshore wind power are marked by red dots.

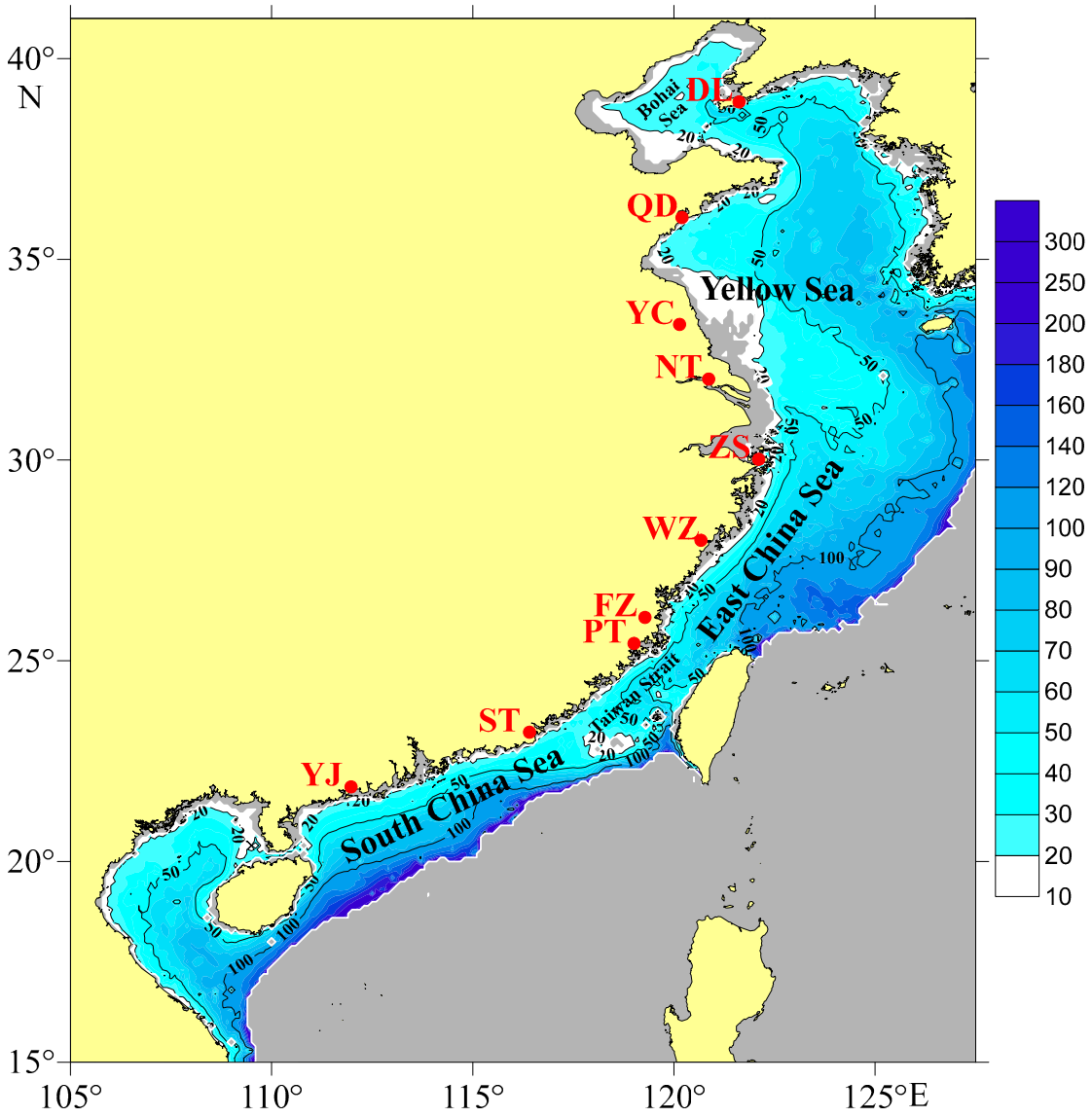

Figure 2. Bathymetry (m) of the waters adjacent to China. The regions (water depth < 10 m and >300 m) are covered by gray. The red dots are cities with massive OWF deployment plans. From south to north, the cities are Yangjiang (YJ), Shantou (ST), Putian (PT), Fuzhou (FZ), Wenzhou (WZ), Zhoushan (ZS), Nantong (NT), Yancheng (YC), Qingdao (QD), and Dalian (DL).

2.2. Basic Equations

We assumed that the water in the study area has an active upper layer (the initial thickness is h_0 and density is ρ) overlying a motionless and infinitely deep layer (the density is $\rho + \Delta\rho$). The vertical coordinate is zero at the sea surface and it is positive in an upward direction. By applying a hydrostatic approximation to the integration of the Navier–Stokes and continuity equations, and by neglecting nonlinear terms, we found that the response of the thickness of the upper layer (h) to wind forcing is

$$\frac{\partial}{\partial t}\left[\left(\frac{\partial^2}{\partial t^2}+f^2\right)h-\nabla\cdot(g'h_0\nabla h)\right]=-\frac{f}{\rho}curl(\tau)-\frac{1}{\rho}\frac{\partial}{\partial t}\nabla\cdot\tau \quad (1)$$

where f is the Coriolis parameter, τ is the wind stress acting on the water column surface, and $g' = g\Delta\rho/\rho$ is the reduced gravity. This equation is valid in a reduced-gravity approximation. It is very general and describes an extensive set of large-/meso-scale marine phenomena which occur in stratified coastal waters [22].

Following the previous work [15], we made two assumptions to simplify Equation (1). First, we neglected the second-order time derivative. This means that all processes of a short time scale ($t < 1/f$, such as internal gravity waves and geostrophic adjustment process) were neglected. Besides, we assumed that the wind forcing is temporally constant; thus, the last term in the right side of Equation (1) was neglected. Then, we transferred all variables in Equation (1) to nondimensional forms. We introduced the scales $(x, y) = (x', y')L$, $t = t' f^{-1}$, and $h = h' \Delta\tau / (\rho f^2 L)$. x and y are the horizontal lengths. $\Delta\tau$ is the deficit of wind stress in the leeward side of the wind turbines. Dropping the primes on the nondimensional variables, the simplified nondimensional Equation (1) is

$$\frac{\partial}{\partial t}\left(h - a^2 \nabla^2 h\right) = -curl\left(\frac{\tau}{\Delta\tau}\right) \tag{2}$$

where $a = \sqrt{g' h_0}/fL$ is the baroclinic Rossby radius ($\sqrt{g' h_0}/f$), divided by the size of the OWFs (L). L is defined as the length scale of OWFs, perpendicular to the wind direction. It should be noticed that the thickness of the upper layer varies linearly over time.

According to the work presented by Broström [15], who first theoretically investigated the effect of OWFs on marine stratifications via large-scale geophysical fluid dynamics, it is difficult to find analytical solutions for Equation (2) if the wind stress force is 2D-variable. However, through the finite element technique, numerical solutions are available, and these indicate that the maximum ocean vertical response depends on the value of a. When all other variables are fixed, the maximum upper layer thickness changes ($h - h_0$ at $t = 1$) as a function of a^2. a is the combination of the width scale of OWFs perpendicular to the wind directions (L), the location (f), and the initial ocean stratification ($g' h_0$). The curve of $\mathcal{F}(a^2)$ (shown in Figure 3 was obtained from the calculation conducted by Broström [15]. The calculation was based on the wind wake, with an idealized 2D form. See [15] for more details.

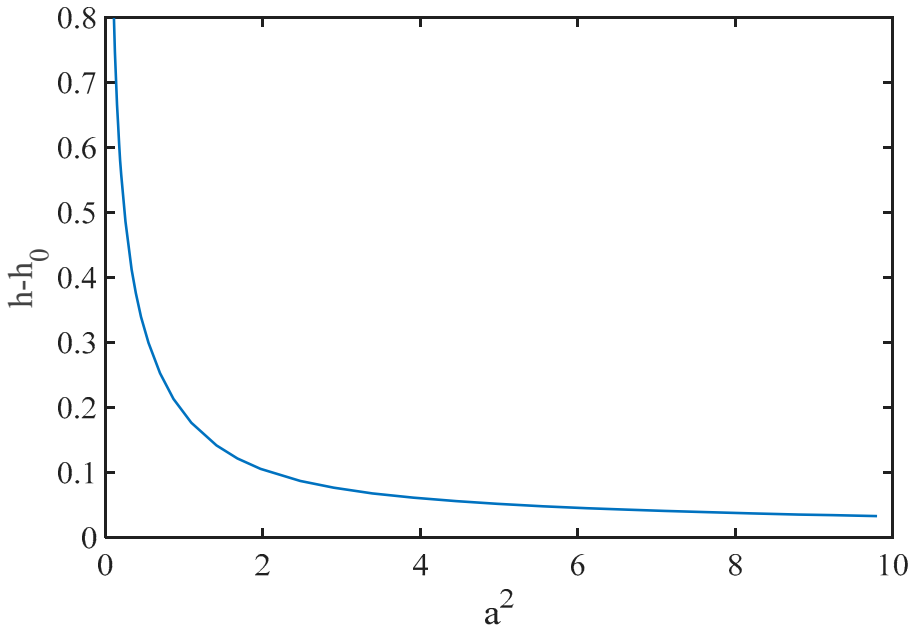

Figure 3. The maximum upper layer thickness changes ($h - h_0$ at $t = 1$) as a function of a^2. This result is digitized from the numerical solutions of Equation (2), as presented by Broström [15] (Reprinted with permission from Ref. [15]. 2008, Elsevier).

Transferring the nondimensional $h - h_0$ back to the dimensional form, we estimated the maximum marine vertical response to the presence of OWFs. The maximum seawater vertical velocity (W) is expected to be

$$W = \frac{\Delta\tau}{\rho f L}\mathcal{F}\left(a^2\right) \tag{3}$$

According to the observations in [21], we set the wind to decrease by 40% due to wind turbines ($\Delta\tau = \tau \times 40\%$). We let $L = 4$ km in the first part of analysis, and we changed L from 3 km to 5 km to investigate the ocean's response to OWFs with different length scales.

2.3. Definition of the Upper Layer Depth (ULD)

The continental shelf of China's adjacent waters is relatively broad and shallow. The ocean temperature is vertically homogeneous, and the stratification disappears in winter due to strong mixing. According to the previous study, the quasi-step-function approximation is suitable for detecting the vertical structures on the Chinese shelf seas [53]. This method introduces three line segments to fit the three layers (surface mixed layer, thermocline, and bottom mixed layer) of the vertical profiles (Figure 4). A quasi-step function can be defined by

$$\begin{cases} T(z) = T_s \\ T(z) = -TS(z - TD) + T_s \\ T(z) = T_b \end{cases} \tag{4}$$

where z is the depth of the profile, T_s and T_b are the vertically averaged temperatures of the surface and bottom mixed layer, TD is the depths of the upper boundary of the thermocline, respectively, and TS is the strength of the thermocline (°C/m). The threshold of the thermocline strength is >0.05 °C/m. If all vertical temperature changes are less than 0.05 °C/m, we considered that the grid is defined by homogeneous vertical mixing. The optimal values of these parameters were calculated through the least-squares adjustment to adjust each temperature profile. We chose the middles of the upper and lower bounds of the thermocline as the bottom of the upper layer, and the thickness between the surface and this level was ULD (h), which was used in the reduced-gravity model.

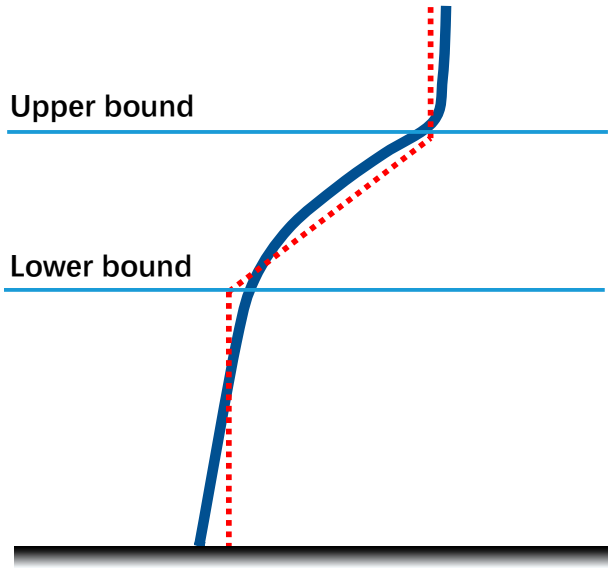

Figure 4. Schematic diagram for the quasi-step-function approximation. The thick blue line indicates the actual vertical temperature profile, the red dash line indicates the fitted three-segment temperature profile. The top and bottom perpendicular segments present the surface and bottom mixed layers; the oblique segment presents the thermocline.

2.4. Data

We used the 2013 version of the World Ocean Atlas (WOA) dataset to identify the ULD and calculated the baroclinic Rossby radius in the waters adjacent to China. The WOA has objectively analyzed climatological mean fields on a quarter-degree longitude by latitude grids [54]. The gridded monthly means of temperature and salinity are on standard levels (0–100 m with 5 m as an increment; 100–300 m with 25 m as an increment).

We chose the quick scatterometer QSCAT/NCEP blended wind product [55] to calculate the wind stress on the sea surface. This data product has a spatial resolution of 0.5 × 0.5 degrees. The variable distributed by this dataset is the wind speed at 10 m height above the sea surface. The wind stress was then calculated according to $\vec{\tau} = \rho * Cd * |\vec{U}| * \vec{U}$, where $\vec{\tau}$ is the wind stress, ρ is the air density (we take 1.3 kg·m^{-3} here), $\vec{U}$ is the wind vector obtained from the product, and Cd is the drag coefficient. In this work, the drag coefficient was calculated using the method suggested by Yelland and Taylor [56]:

$$Cd = \left(0.29 + \frac{3.1}{|\vec{U}|} + \frac{7.7}{|\vec{U}|^2}\right),\ 3\ \text{ms}^{-1} < |\vec{U}| < 6\ \text{ms}^{-1} \quad (5)$$

$$Cd = \left(0.6 + 0.07 * |\vec{U}|\right),\ 6\ \text{ms}^{-1} < |\vec{U}| < 26\ \text{ms}^{-1} \quad (6)$$

Through temporal averaging, the wind stress used in this study was the monthly climatological mean (the original temporal resolution was 6 h, and the available time span was from August 1999 to July 2009).

The study region is 105–127.5 degrees east and 15–41 degrees north. Due to the discrepancy in the spatial grids between the WOA and wind stress product, and for the sake of uniformity, all data were interpolated into a grid with a spatial resolution of 0.1 × 0.1 degree. According to the development planning of OWFs in the waters adjacent to China, most OWFs are going to be built in regions where the water depth is greater than 10 m. Moreover, it is against the economical principle if the OWFs are too far from the coastal line. Therefore, in this study, we only used the grids with a water depth between 10 m and 300 m.

3. Results

3.1. Climatological Mean of Dynamic Marine and Atmosphere Factors

Figure 5 shows that the stratification in the waters adjacent to China is remarkably seasonal. From January to April and in December, most of this region is homogeneously mixed. In May, October, and November, some waters in the shelf are stratified but the coastal waters are mixed well. It is therefore unnecessary to study the ocean's vertical response to OWFs in these regions during these time periods. In contrast, from June to September, the stratified structure is mature and stable in most of the studied waters. This study therefore only investigated the effect of OWFs in these months. During this time, the ULD in the research region generally deepens over time and the deepest ULD occurs in the East China Sea and the north of the South China Sea due to the intrusion of currents from the open seas, such as the Kuroshio Current.

The wind speed within the study domain is also seasonal (Figure 6). The wind speed is large in the East China Sea, especially in the Taiwan Strait, due to the topography effect. According to the energy conversion rate, only the wind speeds higher than 5 m/s (black contour lines in Figure 6) were available for use by OWFs [57]. In June, the wind speed in most of the Bohai Sea and the Yellow Sea was small. The wind-energy-poor regions shrink from south to north over time. Most of the research waters had wind speeds higher than 5 m/s in September.

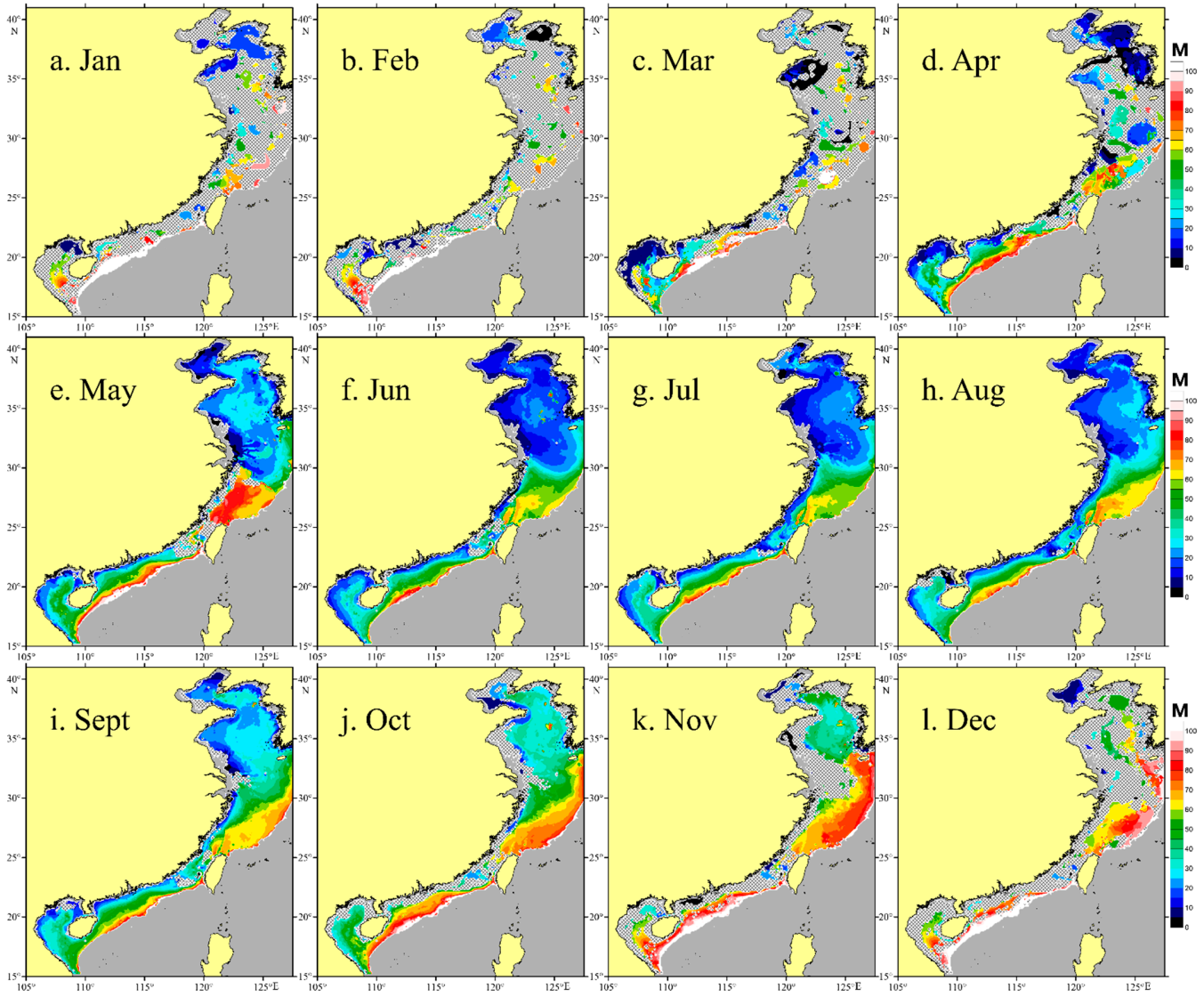

Figure 5. Distribution of ULD (M) in the waters adjacent to China. The regions (water depth < 10 m and >300 m) are covered by gray. The crosshatching indicates the well-mixed regions.

As shown in Equation (2), the baroclinic Rossby radius (R) plays an important role in the effects of OWFs. Figure 7 reveals that R varies dramatically over space and time. Generally, R is small in the nearshore waters and large in the offshore waters. The enlarging of R along with the increase in distance from the seashore is obvious in the East China Sea and the South China Sea shelf where the wind speed is high. For example, to the east of Wenzhou and to the southeast of Yangjiang, R increases from less than 5 km to more than 20 km within 50 NM. It should be noted that there are exceptions between Wenzhou and Shantou. Here, the area with small R spreads relatively far towards the offshore waters. The conditions in the Bohai Sea and the Yellow Sea are different. The area with small R is large and widespread, but the wind speed in these waters is relatively low, particularly in June and July.

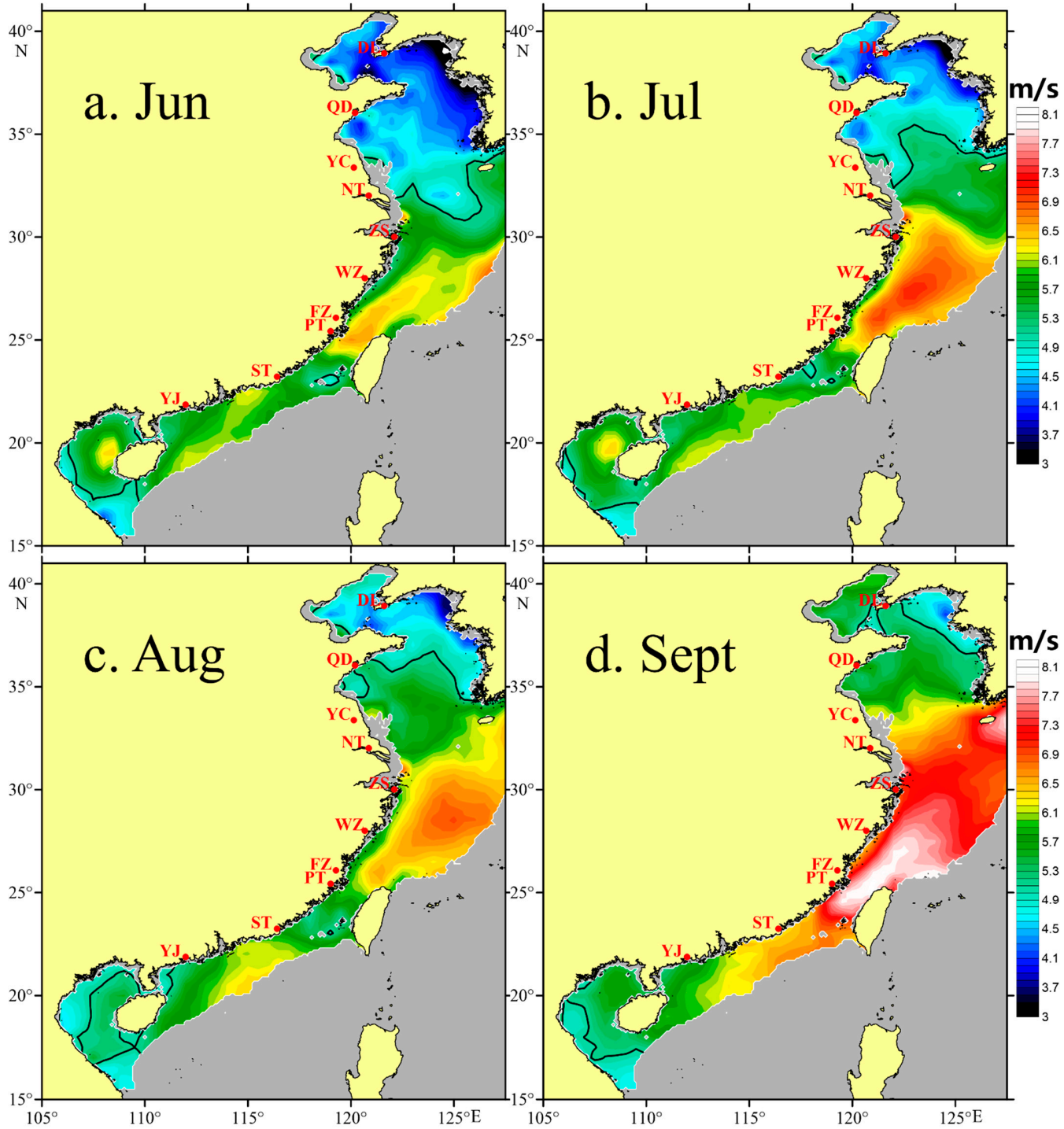

Figure 6. Distribution of wind speed (m/s) in the waters adjacent to China. The black lines indicate the contour lines with a wind speed of 5 m/s.

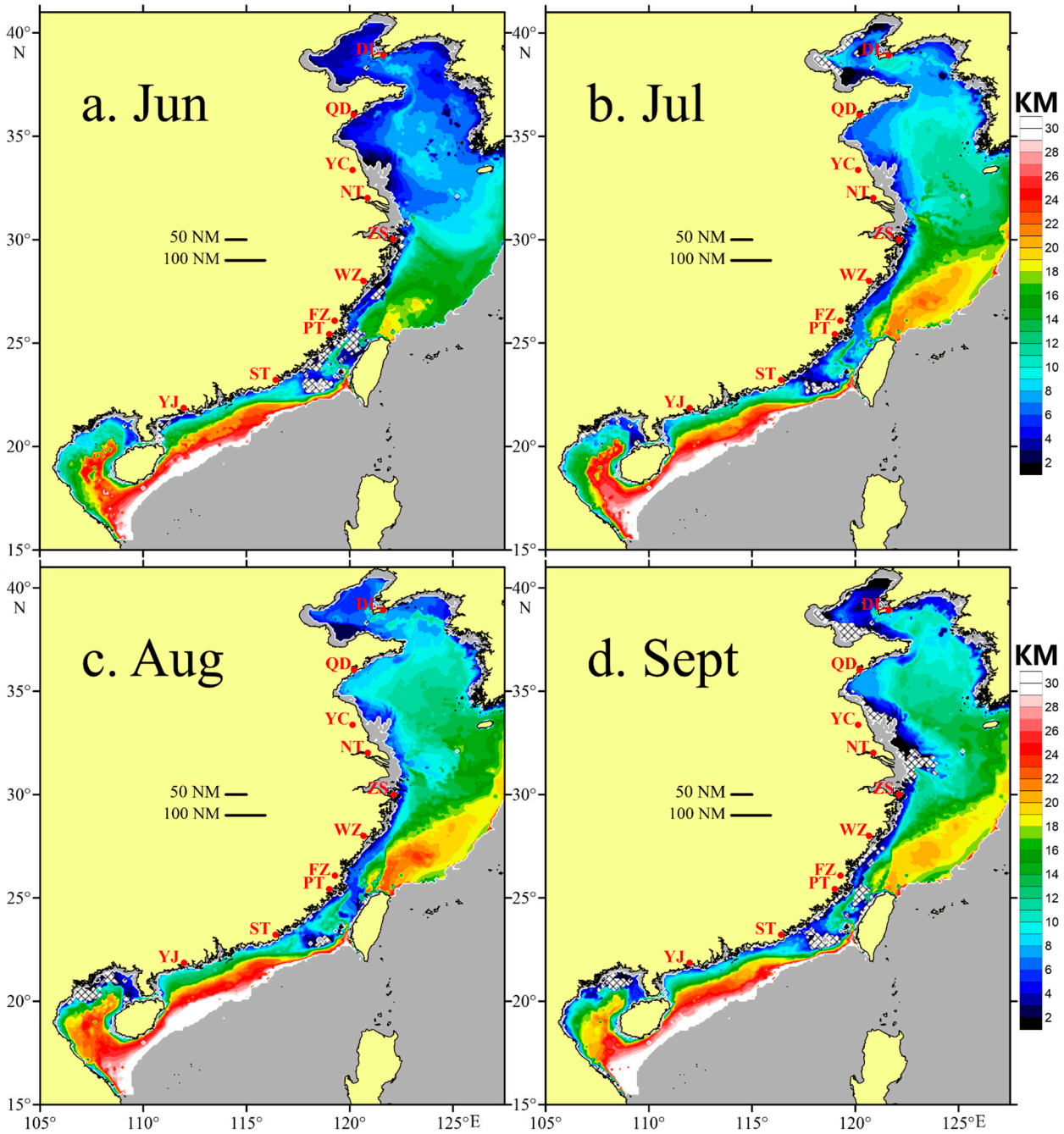

Figure 7. Distribution of the baroclinic Rossby radius (KM) in the waters adjacent to China. The two horizontal black bars indicate reference lengths of 50 NM and 100 NM, respectively. The crosshatching indicates the regions without stratification.

3.2. Impact of OWFs Layout on Marine Stratification

Based on the calculations, the triggered W is presented in Figure 8. The potential ocean dynamic response to the OWFs varies spatially. The W values are large near the coastal lines and are small far away from the seashore. The maximum magnitude of velocity can reach as high as more than 1 m/d. This is a joint result induced by the original background ocean stratification and the wind force. During summertime, the adjacent waters in China are affected by southerly winds. Because of the associated offshore Ekman transport, there are upwelling systems near the coastal lines. The marine stratification is therefore weak in these regions which leads to a small a. Combined with a large τ, the W is then relatively large near the coast.

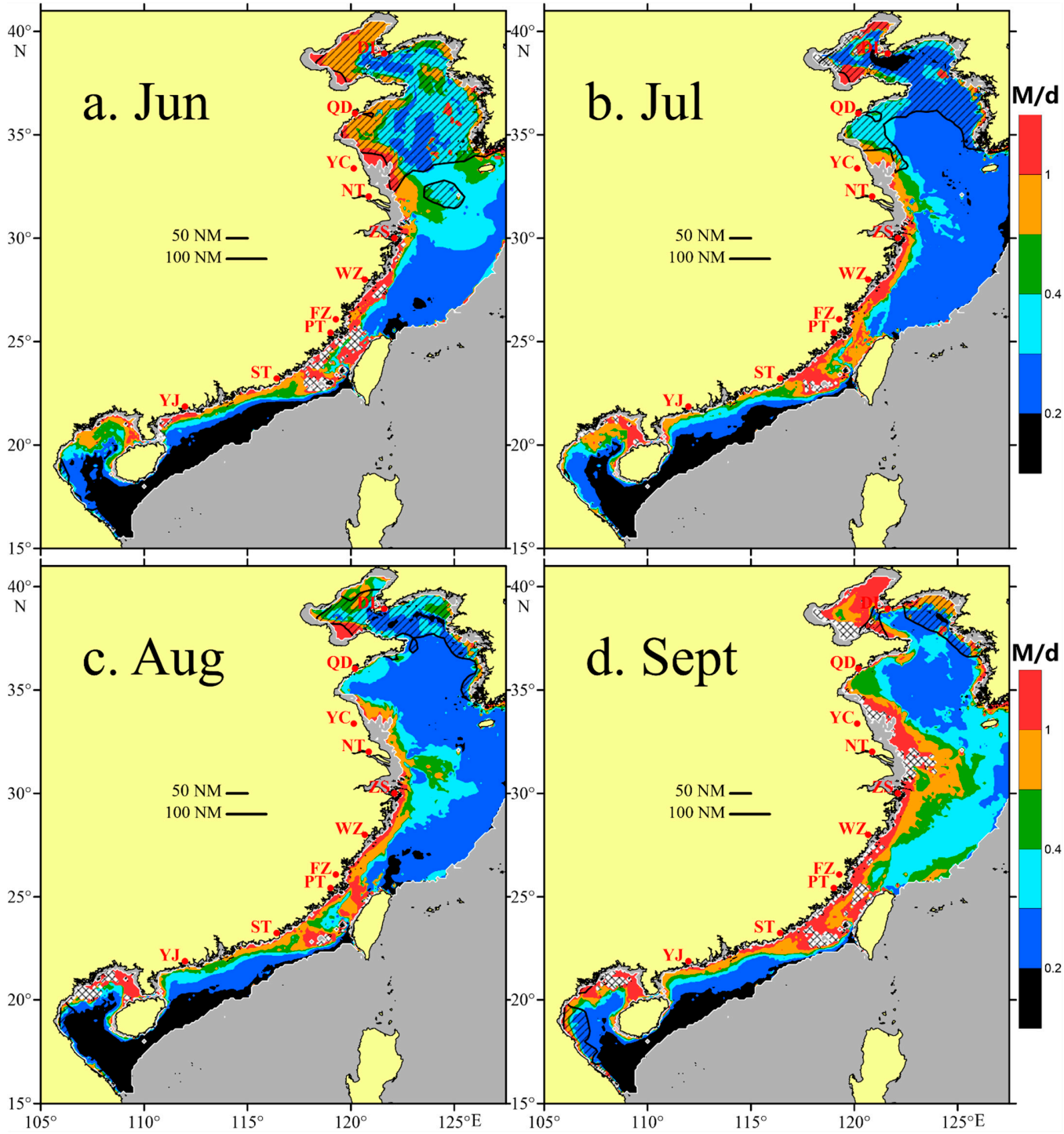

Figure 8. Distribution of the maximum seawater vertical velocity (M/d) in the waters adjacent to China. The two horizonal black bars indicate reference lengths of 50 NM and 100 NM, respectively. The regions covered by slashes are of wind speed less than 5 m/s. The crosshatching indicates the regions without stratification.

There are several hotspots for the effect of OWFs. The first one is the Taiwan Strait. In all months, from Fuzhou to Shantou, on the one hand, the wind energy is the most abundant in the study region. On the other hand, in these waters, the area with strong vertical velocity (>0.5 m/d) is large, suggesting that the ocean vertical response is particularly sensitive to the OWFs. In waters about 100 NM away from the mainland within this region, the W is still larger than 1 m/d. The other hotspots are not typical in all stratified months. For

example, the region to the east of Zhoushan and Nantong and the Bohai Sea have significant ocean dynamic response in September only, and the regions with large W (~1 m/d) extend from the coast by around 100 NM. This is because, despite the fact that weak stratification facilitates a large ocean response, the wind speed is too slow to induce strong vertical velocity in July and August.

There are some regions where the situation is different. To the southeast of Yangjiang, the ocean is insensitive to OWFs, and the potential velocity dramatically decreases as the distance from the coast increases. In June, the Bohai Sea and the Yellow Sea begin to stratify. The ULD is therefore very thin and the vertical density changes are small. The potential vertical velocity is thus significant despite the low wind speed. The operational days of wind turbines in these regions might be short in June; thus, their influences need to be evaluated further, despite the potentially large magnitude of the induced velocity.

To investigate the impact of OWFs on the marine vertical structure, we calculate the time needed to raise the bottom of the upper layer to the sea surface ($T = ULD/W$, Figure 9). The pattern of T is generally consistent with that of W. In the regions with large W, the original marine stratification would be easily destroyed (<10 days) due to the deployment of OWFs. This estimation is rough, and some effects (frictions, nonlinearity) have been neglected. The actual stratification-breaking time must be, to some degree, longer than this estimation. However, this result still suggests that OWFs are most likely to play important roles in the marine stratifications of the hotspot regions.

It is also worth investigating the ocean's sensitivity to the length scale of the OWFs perpendicular to the wind direction (L). On the one hand, the increase in L will reduce W according to Equation (3). On the other hand, a large L leads to a small a but a large $\mathcal{F}(a^2)$, leading to an eventual increase in W. Calculation reveals that (Figure 10), along with the increase in L, the decrease in W mainly occurs near the coast to the south of Zhoushan. On contrary, in the waters further away from the seashore by around 30 NM, broader OWFs would induce larger ocean vertical velocity. To the north of Zhoushan, it is mainly the increasing effect working, and W generally increases when L increases in June, July, and August.

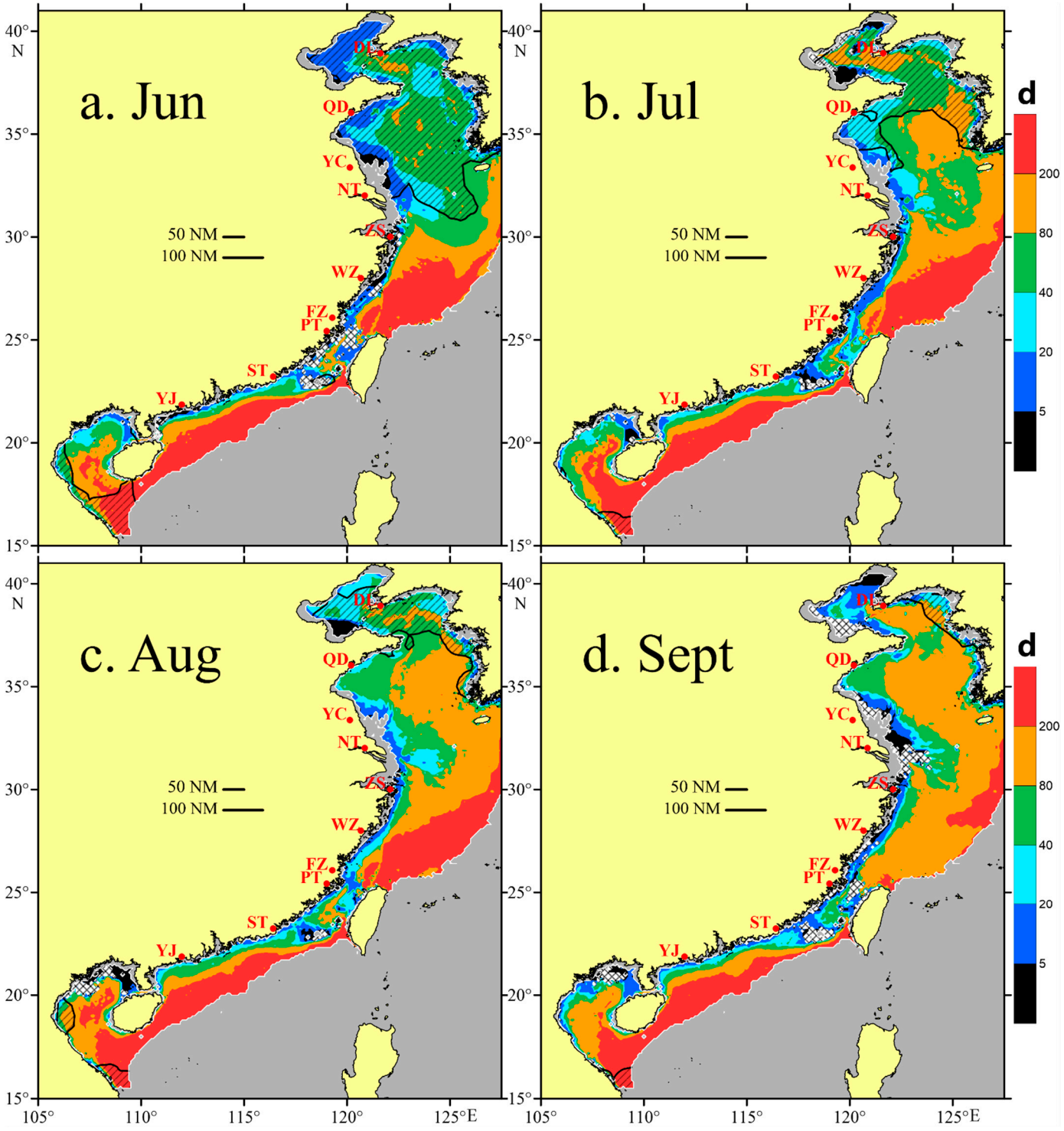

Figure 9. Distribution of the days of the background ocean stratification destroyed (d) in the waters adjacent to China. The two horizonal black bars indicate reference lengths of 50 NM and 100 NM, respectively. The regions covered by slashes are of wind speed less than 5 m/s. The crosshatching indicates the regions without stratification.

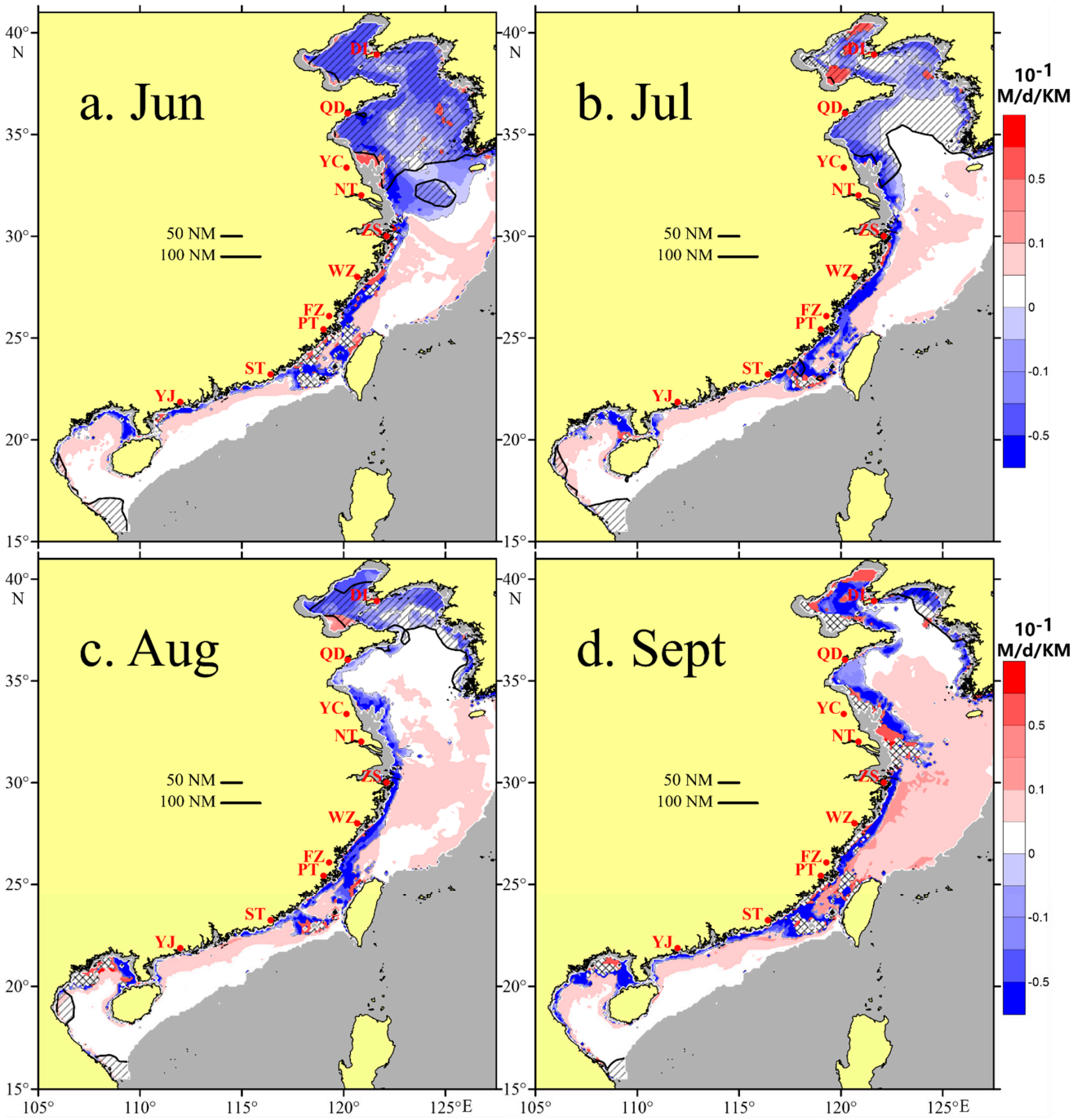

Figure 10. Distribution of the rate of W changing (10^{-1} M/d/KM) due to an increase in L in the waters adjacent to China. The two horizontal black bars indicate reference lengths of 50 NM and 100 NM, respectively. The regions covered by slashes are of wind speed of less than 5 m/s. The crosshatching indicates the regions without stratification.

4. Conclusions and Discussions

The theoretical calculations presented here exhibit the geographical patterns of the dynamic marine responses to OWFs in the waters adjacent to China. According to the pattern, there are two suggestions for the planning of OWF deployments. The first suggestion concerns the locations of the OWFs. In the stratified seasons (from June to September), inshore waters have a strong vertical dynamic response to OWFs. In particular, there are two hotspots of OWF impact, which are regions between Fuzhou and Shantou, and are to the east of Zhoushan and Nantong. The areas with large, triggered velocities spread

eastward by around 100 NM. In the hotspots, the original stratifications would be altered with a high efficiency compared with the quiet areas. These dramatic spatial differences suggest that the OWF deployment plan in the hotspots is needed to consider the impacts on the marine stratifications. Secondly, this analysis provides suggestions for how to choose suitable length scales for OWFs in different waters. For the regions with abundant wind energy, the ocean vertical response to the increase in OWF width is opposite in the coastal waters versus the open seas. The boundary is about 30 NM from the mainland coast. To the east of Fuzhou, Putian, and Shantou, the regions with decreasing velocities are relatively broad. Therefore, if the designers of the OWFs in these regions prefer a larger ocean vertical response, then a broader OWF should be a suitable choice.

The main outcomes of this study are the presentation of the geographical patterns of ocean responses to OWFs in the waters adjacent to China. The presented pattern is physically meaningful and compelling. It is logical from the perspective of geophysical fluid dynamics. The pattern is mainly caused by the combination of background stratification and wind force. In the hotspot regions, both of the factors (strong wind and weak stratification) favor the increase in marine sensitivity to OWFs. Consequently, abstracting the characteristic scales from the waters adjacent to China and implementing scales using geophysical fluid equations can address the issue which is the focus of this study. In summary, we derived the basic characteristic of the impacts of OWFs on marine stratification, rather than the exact vertical velocity, as reflected by the computation.

The deficiency in this purely theoretical estimation is obvious and non-negligible. First, there are many factors which play roles in regulating the effect of OWFs on marine stratification. For instance, in the current theoretical framework, we assumed that wind force is constant over time; thus, the calculation cannot determine the ocean's response to time-variable winds. Similarly, the nonlinear and friction effects were also excluded in this study. Due to enhancing vertical mixing, a strong wind force may weaken stratification, additionally inducing large vertical velocity. These effects are incompatible with the current linear method. Lastly, the parameters used in the research alter the estimations, and the values of these parameters, such as the wind deficit within the atmospheric wake behind turbines and the length scales of individual OWFs, have a wide range. For instance, there are observations showing that the wind speeds in the wakes are in the range of 7–8 m/s and the free-stream wind speeds are in the range of 9–10 m/s [58]. According to a wake theory, the maximum wind reduction reaches 80% [11]. The lengths of OWFs widely range from 10^0 km to 10^1 km [59]. There are various values for these factors; however, this study aimed to present macroscopic features of the influences of OWFs on marine stratification; therefore, the final outcomes do not depend on specific parameter values.

The influence of OWFs on the marine environment must be profound. On the one hand, the dynamic consequence of the changes in marine stratification is complex. Once OWFs change the original state of marine vertical stability, the associated variability of the pressure gradient force might interact with the surrounding circulations; thus, the pathway and magnitude of coastal currents and diluted water may change. On the other hand, the corresponding marine ecological response is also likely to occur in the study areas. The months when OWFs lead to strong vertical seawater movements are in the summertime. In this season, the environmental factors in most of the studied waters were found to be suitable for the reproduction and growth of marine organisms. From the perspective of the possibility of marine carbon sequestration, the time window of the effects on marine stratification is beneficial in highlighting the low-carbon features of the offshore wind industry in the studied waters. Moreover, there are some traditional fishing grounds in the OWF-hotspot waters, such as Zhoushan fishing ground (to the east of Zhoushan) and Yuedong fishing ground (to the east of Shantou). The background marine ecosystems here are productive and complex. Detailed investigations into the effects of OWFs on local marine ecosystems is necessary in the future.

In summary, for the first time, this study highlights the potential importance of the impacts of OWFs on marine stratification in the waters adjacent to China. Although

the estimation is qualitative rather than quantitative, this study lays the foundations for understanding the marine dynamic environmental effects of OWFs around China. The time evolution and 3D ocean response to the different OWF deployment plans will be conducted using numerical models in the next study. Thus, the effects of extreme and short-term events, such as typhoons and diurnal variations, can be evaluated in detail.

Author Contributions: Conceptualization, Z.L.; methodology, Z.L.; software, K.L.; validation, K.L.; formal analysis, T.Y.; investigation, Z.L.; resources, Z.L.; data curation, T.Y.; writing—original draft, K.L.; writing—review and editing, Z.L.; visualization, K.L., T.Y. and Z.L.; supervision, Z.L.; project administration, Z.L.; funding acquisition, Z.L. All authors have read and agreed to the published version of the manuscript.

Funding: This work was supported by the Shantou University Scientific Research Funded Project [grant number NTF21009], the MEL Visiting Fellowship [grant number MELRS2118].

Institutional Review Board Statement: Not applicable.

Informed Consent Statement: Not applicable.

Data Availability Statement: Not applicable.

Conflicts of Interest: The authors declare no conflict of interest.

References

1. Esteban, M.D.; Diez, J.J.; López, J.S.; Negro, V. Why offshore wind energy? *Renew. Energy* **2011**, *36*, 444–450. [CrossRef]
2. Díaz, H.; Guedes Soares, C. Review of the current status, technology and future trends of offshore wind farms. *Ocean Eng.* **2020**, *209*, 107381. [CrossRef]
3. Fan, Q.; Wang, X.; Yuan, J.; Liu, X.; Hu, H.; Lin, P. A Review of the Development of Key Technologies for Offshore Wind Power in China. *J. Mar. Sci. Eng.* **2022**, *10*, 929. [CrossRef]
4. Hall, R.; Topham, E.; João, E. Environmental Impact Assessment for the decommissioning of offshore wind farms. *Renew. Sustain. Energy Rev.* **2022**, *165*, 112580. [CrossRef]
5. Ivanov, E.; Capet, A.; De Borger, E.; Degraer, S.; Delhez, E.J.M.; Soetaert, K.; Vanaverbeke, J.; Grégoire, M. Offshore Wind Farm Footprint on Organic and Mineral Particle Flux to the Bottom. *Front. Mar. Sci.* **2021**, *8*, 631799. [CrossRef]
6. Slavik, K.; Lemmen, C.; Zhang, W.; Kerimoglu, O.; Klingbeil, K.; Wirtz, K.W. The large-scale impact of offshore wind farm structures on pelagic primary productivity in the southern North Sea. *Hydrobiologia* **2019**, *845*, 35–53. [CrossRef]
7. Jiao, N.; Liu, J.; Jiao, F.; Chen, Q.; Wang, X. Microbes mediated comprehensive carbon sequestration for negative emission in the ocean. *Natl. Sci. Rev.* **2020**, *7*, 1858–1860. [CrossRef]
8. Jiao, N.; Cai, R.; Zheng, Q.; Tang, K.; Liu, J.; Jiao, F.; Wallace, D.; Chen, F.; Li, C.; Amann, R.; et al. Unveiling the enigma of refractory carbon in the ocean. *Natl. Sci. Rev.* **2018**, *5*, 459–463. [CrossRef]
9. Worden, A.Z.; Follows, M.J.; Giovannoni, S.J.; Wilken, S.; Zimmerman, A.E.; Keeling, P.J. Rethinking the marine carbon cycle: Factoring in the multifarious lifestyles of microbes. *Science* **2015**, *347*, 1257594. [CrossRef]
10. Cazenave, P.W.; Torres, R.; Allen, J.I. Unstructured grid modelling of offshore wind farm impacts on seasonally stratified shelf seas. *Prog. Oceanogr.* **2016**, *145*, 25–41. [CrossRef]
11. Frandsen, S. On the wind speed reduction in the center of large clusters of wind turbines. *J. Wind Eng. Ind. Aerodyn.* **1992**, *39*, 251–265. [CrossRef]
12. Christiansen, M.B.; Hasager, C.B. Wake effects of large offshore wind farms identified from satellite SAR. *Remote Sens. Environ.* **2005**, *98*, 251–268. [CrossRef]
13. Frandsen, S.; Barthelmie, R.; Pryor, S.; Rathmann, O.; Larsen, S.; Højstrup, J.; Thøgersen, M. Analytical modelling of wind speed deficit in large offshore wind farms. *Wind Energy* **2006**, *9*, 39–53. [CrossRef]
14. Zhao, L.; Xue, L.; Li, Z.; Wang, J.; Yang, Z.; Xue, Y. Progress on Offshore Wind Farm Dynamic Wake Management for Energy. *J. Mar. Sci. Eng.* **2022**, *10*, 1395. [CrossRef]
15. Broström, G. On the influence of large wind farms on the upper ocean circulation. *J. Mar. Syst.* **2008**, *74*, 585–591. [CrossRef]
16. Ahsbahs, T.; Badger, M.; Volker, P.; Hansen, K.S.; Hasager, C.B. Applications of satellite winds for the offshore wind farm site Anholt. *Wind Energy Sci.* **2018**, *3*, 573–588. [CrossRef]
17. Nygaard, N.G.; Newcombe, A.C. Wake behind an offshore wind farm observed with dual-Doppler radars. *J. Phys. Conf. Ser.* **2018**, *1037*, 072008. [CrossRef]
18. Cañadillas, B.; Foreman, R.; Barth, V.; Siedersleben, S.; Lampert, A.; Platis, A.; Djath, B.; Schulz-Stellenfleth, J.; Bange, J.; Emeis, S.; et al. Offshore wind farm wake recovery: Airborne measurements and its representation in engineering models. *Wind Energy* **2020**, *23*, 1249–1265. [CrossRef]
19. Van der Hoven, I. Power sprecturm of horizontal wind speed in the frequency range from 0.0007 to 900 cycles per hour. *J. Atmos. Sci.* **1957**, *14*, 160–164. [CrossRef]

20. Ludewig, E. *On the Effect of Offshore Wind Farms on the Atmosphere and Ocean Dynamics*; Springer: Berlin/Heidelberg, Germany, 2015.
21. Platis, A.; Siedersleben, S.K.; Bange, J.; Lampert, A.; Bärfuss, K.; Hankers, R.; Cañadillas, B.; Foreman, R.; Schulz-Stellenfleth, J.; Djath, B. First in situ evidence of wakes in the far field behind offshore wind farms. *Sci. Rep.* **2018**, *8*, 2163. [CrossRef]
22. Pedlosky, J. *Geophysical Fluid Dynamics*; Springer: Berlin/Heidelberg, Germany, 1987; Volume 710.
23. Lange, M.; Burkhard, B.; Garthe, S.; Gee, K.; Kannen, A.; Lenhart, H.; Windhorst, W. *Analyzing Coastal and Marine Changes: Offshore Wind Farming as a Case Study, 1383–4304*; GKSS Research Center: Geesthacht, Germany, 2010; p. 212.
24. Paskyabi, M.B.; Fer, I. Upper Ocean Response to Large Wind Farm Effect in the Presence of Surface Gravity Waves. *Energy Procedia* **2012**, *24*, 245–254. [CrossRef]
25. Afsharian, S.; Taylor, P.A. On the Potential Impact of Lake Erie Wind Farms on Water Temperatures and Mixed-Layer Depths: Some Preliminary 1-D Modeling Using COHERENS. *J. Geophys. Res. Ocean.* **2019**, *124*, 1736–1749. [CrossRef]
26. Floeter, J.; van Beusekom, J.E.E.; Auch, D.; Callies, U.; Carpenter, J.; Dudeck, T.; Eberle, S.; Eckhardt, A.; Gloe, D.; Hänselmann, K.; et al. Pelagic effects of offshore wind farm foundations in the stratified North Sea. *Prog. Oceanogr.* **2017**, *156*, 154–173. [CrossRef]
27. Floeter, J.; Pohlmann, T.; Harmer, A.; Möllmann, C. Chasing the offshore wind farm wind-wake-induced upwelling/downwelling dipole. *Front. Mar. Sci.* **2022**, *9*, 1390. [CrossRef]
28. Fennel, W.; Lass, H.U. On the impact of wind curls on coastal currents. *J. Mar. Syst.* **2007**, *68*, 128–142. [CrossRef]
29. Albert, A.; Echevin, V.; Lévy, M.; Aumont, O. Impact of nearshore wind stress curl on coastal circulation and primary productivity in the Peru upwelling system. *J. Geophys. Res. Ocean.* **2010**, *115*. [CrossRef]
30. Farr, H.; Ruttenberg, B.; Walter, R.K.; Wang, Y.-H.; White, C. Potential environmental effects of deepwater floating offshore wind energy facilities. *Ocean Coast. Manag.* **2021**, *207*, 105611. [CrossRef]
31. Okkonen, S.; Niebauer, H. Ocean circulation in the Bering Sea marginal ice edge zone from Acoustic Doppler Current Profiler observations. *Cont. Shelf Res.* **1995**, *15*, 1879–1902. [CrossRef]
32. Foreman, R.; Cañadillas, B.; Neumann, T.; Emeis, S. Measurements of heat and humidity fluxes in the wake of offshore wind turbines. *J. Renew. Sustain. Energy* **2017**, *9*, 053304. [CrossRef]
33. Paskyabi, M.B. Offshore Wind Farm Wake Effect on Stratification and Coastal Upwelling. *Energy Procedia* **2015**, *80*, 131–140. [CrossRef]
34. Carpenter, J.R.; Merckelbach, L.; Callies, U.; Clark, S.; Gaslikova, L.; Baschek, B. Potential impacts of offshore wind farms on North Sea stratification. *PLoS ONE* **2016**, *11*, e0160830. [CrossRef] [PubMed]
35. Siedersleben, S.K.; Lundquist, J.K.; Platis, A.; Bange, J.; Bärfuss, K.; Lampert, A.; Cañadillas, B.; Neumann, T.; Emeis, S. Micrometeorological impacts of offshore wind farms as seen in observations and simulations. *Environ. Res. Lett.* **2018**, *13*, 124012. [CrossRef]
36. Mallapaty, S. How China could be carbon neutral by mid-century. *Nature* **2020**, *586*, 482–483. [CrossRef]
37. Zhang, S.; Wei, J.; Chen, X.; Zhao, Y. China in global wind power development: Role, status and impact. *Renew. Sustain. Energy Rev.* **2020**, *127*, 109881. [CrossRef]
38. Global Wind Energy Council. *GWEC Global Wind Report 2019*; Global Wind Energy Council: Brussels, Belgium, 2019.
39. Notice on the Development Strategy of Offshore Wind Farms in Guangdong Issued by Guangdong Provincial on Development and Reform Commission. Available online: http://drc.gd.gov.cn/gkmlpt/content/1/1060/post_1060661.html#876 (accessed on 26 October 2022).
40. Yang, Q.; Chen, G.Q.; Liao, S.; Zhao, Y.H.; Peng, H.W.; Chen, H.P. Environmental sustainability of wind power: An emergy analysis of a Chinese wind farm. *Renew. Sustain. Energy Rev.* **2013**, *25*, 229–239. [CrossRef]
41. Leung, D.Y.C.; Yang, Y. Wind energy development and its environmental impact: A review. *Renew. Sustain. Energy Rev.* **2012**, *16*, 1031–1039. [CrossRef]
42. Chang, K.-T.; Jeng, D.-S. Numerical study for wave-induced seabed response around offshore wind turbine foundation in Donghai offshore wind farm, Shanghai, China. *Ocean Eng.* **2014**, *85*, 32–43. [CrossRef]
43. Wang, T.; Ru, X.; Deng, B.; Zhang, C.; Wang, X.; Yang, B.; Zhang, L. Evidence that offshore wind farms might affect marine sediment quality and microbial communities. *Sci. Total Environ.* **2023**, *856*, 158782. [CrossRef]
44. Wang, T.; Yu, W.; Zou, X.; Zhang, D.; Li, B.; Wang, J.; Zhang, H. Zooplankton Community Responses and the Relation to Environmental Factors from Established Offshore Wind Farms within the Rudong Coastal Area of China. *J. Coast. Res.* **2017**, *34*, 843–855. [CrossRef]
45. Wang, T.; Zou, X.; Li, B.; Yao, Y.; Li, J.; Hui, H.; Yu, W.; Wang, C. Microplastics in a wind farm area: A case study at the Rudong Offshore Wind Farm, Yellow Sea, China. *Mar. Pollut. Bull.* **2018**, *128*, 466–474. [CrossRef]
46. Huang, C.-T.; Afero, F.; Hung, C.-W.; Chen, B.-Y.; Nan, F.-H.; Chiang, W.-S.; Tang, H.-J.; Kang, C.-K. Economic feasibility assessment of cage aquaculture in offshore wind power generation areas in Changhua County, Taiwan. *Aquaculture* **2022**, *548*, 737611. [CrossRef]
47. Wang, J.; Zou, X.; Yu, W.; Zhang, D.; Wang, T. Effects of established offshore wind farms on energy flow of coastal ecosystems: A case study of the Rudong offshore wind farms in China. *Ocean Coast. Manag.* **2019**, *171*, 111–118. [CrossRef]
48. Yang, J.; Chang, Y.; Zhang, L.; Hao, Y.; Yan, Q.; Wang, C. The life-cycle energy and environmental emissions of a typical offshore wind farm in China. *J. Clean. Prod.* **2018**, *180*, 316–324. [CrossRef]
49. Li, H.; Jiang, H.-D.; Dong, K.-Y.; Wei, Y.-M.; Liao, H. A comparative analysis of the life cycle environmental emissions from wind and coal power: Evidence from China. *J. Clean. Prod.* **2020**, *248*, 119192. [CrossRef]

50. Xu, J.; Zhang, R.; Wang, Y.; Yan, H.; Liu, Q.; Guo, Y.; Ren, Y. A New Framework for Assessment of Offshore Wind Farm Location. *J. Mar. Sci. Eng.* **2022**, *15*, 6758. [CrossRef]
51. Make, M.; Vaz, G. Analyzing scaling effects on offshore wind turbines using CFD. *Renew. Energy* **2015**, *83*, 1326–1340. [CrossRef]
52. Yang, D.; Meneveau, C.; Shen, L. Large-eddy simulation of offshore wind farm. *Phys. Fluids* **2014**, *26*, 025101. [CrossRef]
53. Hao, J.; Chen, Y.; Wang, F.; Lin, P. Seasonal thermocline in the China Seas and northwestern Pacific Ocean. *J. Geophys. Res. Ocean.* **2012**, *117*. [CrossRef]
54. Locarnini, R.A.; Mishonov, A.V.; Antonov, J.I.; Boyer, T.P.; Garcia, H.E.; Baranova, O.K.; Zweng, M.M.; Paver, C.R.; Reagan, J.R.; Johnson, D.R.; et al. *World Ocean Atlas 2013, Volume 1: Temperature*; NOAA Atlas NESDIS 73; Ocean Climate Laboratory, National Oceanographic Data Center: Washington, DC, USA, 2013; p. 40.
55. Colorado Research Associates/Northwest Research Associates/Inc. *N.R. QSCAT/NCEP Blended Ocean Winds from Colorado Research Associates (Version 5.0)*, Research Data Archive at the National Center for Atmospheric Research, Computational and Information Systems Laboratory: Boulder, CO, USA, 1999–2009. Available online: http://rda.ucar.edu/datasets/ds744.4/(accessed on 4 October 2021).
56. Yelland, M.; Taylor, P.K. Wind Stress Measurements from the Open Ocean. *J. Phys. Oceanogr.* **1996**, *26*, 541–558. [CrossRef]
57. Zheng, C.W.; Pan, J. Assessment of the global ocean wind energy resource. *Renew. Sustain. Energy Rev.* **2014**, *33*, 382–391. [CrossRef]
58. Larsén, X.G.; Fischereit, J. A case study of wind farm effects using two wake parameterizations in the Weather Research and Forecasting (WRF) model (V3.7.1) in the presence of low-level jets. *Geosci. Model. Dev.* **2021**, *14*, 3141–3158. [CrossRef]
59. Zhang, T.; Tian, B.; Sengupta, D.; Zhang, L.; Si, Y. Global offshore wind turbine dataset. *Sci. Data* **2021**, *8*, 191. [CrossRef] [PubMed]